Journal of Materials Chemistry A

ROYAL SOCIETY OF CHEMISTRY

PAPER

View Article Online
View Journal | View Issue

Check for updates

Cite this: J. Mater. Chem. A, 2025, 13, 37063

Phosphorylated carbon cathodes achieve perfect monovalent cation selectivity in capacitive deionization

Ankita Mathur, [ab] Sally Nijem,[a] Rana Uwayid, [b] Zohar Sahray,[b] Amit N. Shocron, [ab] Matthew E. Suss*[bcd] and Charles E. Diesendruck *[ac]

Received 26th June 2025
Accepted 4th August 2025

DOI: 10.1039/d5ta05182g

rsc.li/materials-a

Selective sodium removal from water sources is crucial for irrigation and other applications, yet challenging due to the abundance of sodium ions compared to essential minerals like calcium and magnesium. Capacitive deionization (CDI) is an emerging electrochemical technique for water treatment and desalination which uses a small electrical potential to adsorb ions in the double layers of microporous electrodes. Given the micropore size is of the same order of magnitude as hydrated ions, CDI offers potential for ion differentiation based on properties such as charge, radius, diffusion constant, and more. Herein, the development of monovalent selective CDI through surface modification of activated carbon cathodes with phosphoric acid groups is described. Cathode phosphorylation induces negative surface charges within the micropores, resulting in enhanced absorption of smaller sodium ions and no calcium uptake during CDI. By applying short, alternating charge–discharge cycles, this membraneless system achieves perfect monovalent cation selectivity with low energy consumption (as low as 0.28 kWh m^{-3}), removing sodium from the water without reducing the calcium concentration.

Introduction

The growing global population and increasing freshwater scarcity have made wastewater and seawater purification essential for securing potable water supplies, as well as providing treated water for irrigation and industrial uses.[1,2] Beyond targeting an overall reduction in ionic strength, the selective removal of specific ions is essential for various applications, such as the removal of heavy metals from wastewater; removal of Na^+ for irrigation; attaining and recovering precious metals like gold and lithium; or controlling water hardness by removal of mineral ions from wastewater.[3–5] Many large water sources (*e.g.* brackish water) remain underutilized due to excessive Na^+ concentrations, which can be detrimental to soil health and various industrial processes. In particular, irrigation requires removal of excess Na^+ to preserve crop yields, soil quality and water infiltration rates.[6] Indeed, amongst different parameters, irrigation water quality is defined by its ionic conductivity and sodium adsorption ratio (SAR), which quantifies the ratio between Na^+ and (Mg^{2+} + Ca^{2+}) concentrations. Yet, achieving selective removal of specific monovalent cations in a multi-ion feed is challenging, particularly when it is desirable to retain multivalent ions such as Ca^{2+} and Mg^{2+}.[7,8] Among the monovalent cations, Na^+ ions are often present at considerably higher concentrations compared to other minerals, and their selective removal is particularly important due to their pronounced impacts on soil quality, human and animal health, and various industrial applications. Notably, selectivity in monovalent cation separation is also critical for recovering valuable ions such as Li^+, which is increasingly in demand for the battery industry.[9] Moreover, for applications in agriculture and human health, the selective retention of potassium (K^+) – generally found at low concentrations in natural waters – is important, as unintentional removal could have detrimental effects.

Conventional ion-selective water purification technologies such as nanofiltration and electrodialysis (ED) inherently favor multivalent ion separation as a consequence of stronger electrostatic interactions.[10,11] While monovalent-selective ED has been achieved by layering membranes with polyelectrolytes, such treatment reduces membrane conductivity and lifetime.[12] Similarly, adding a charged layer to the feed side of the nanofiltration membrane can enhance monovalent or divalent ion selectivity, but this system needs to be tailored to each feedwater composition or changes in effluent requirements.[13,14] Therefore, the development of inherently ion-selective water purification technologies represents a crucial next step in the

[a]Schulich Faculty of Chemistry, Technion – Israel Institute of Technology, Haifa, 3200008, Israel. E-mail: charles@technion.ac.il

[b]Faculty of Mechanical Engineering, Technion – Israel Institute of Technology, Haifa, 3200003, Israel. E-mail: mesuss@me.technion.ac.il

[c]Grand Technion Energy Program, Technion – Israel Institute of Technology, Haifa, 3200003, Israel

[d]Wolfson Department of Chemical Engineering, Technion – Israel Institute of Technology, 3200003, Haifa, Israel

field, offering the potential to produce treated water that is less dependent on feedwater ion composition, and can also be directly tuned towards different effluent compositions.

Capacitive deionization (CDI) has been gaining recognition as a promising low-energy alternative to membrane-based technologies for ion-selective separations, particularly in the context of sustainable water treatment and reuse.[4] Within the growing clean water-energy nexus, achieving precise ionic separations without sacrificial trade-offs in conductivity or energy demand remains a core challenge. CDI is a membraneless electrochemical technique that applies low voltage (typically around 1 V) across a pair of porous electrodes separated by a dielectric separator.[15,16] During the charging step, ions migrate from the solution and are held electrostatically in the electrodes, often in electric double layers (EDLs) that form within the electrode micropores.[17] Once charged, the electrodes can be discharged to desorb the stored ions and regenerate the electrode, resulting in a concentrated brine effluent. CDI systems with engineered electrode chemistries hold significant promise for achieving ion selectivity, due to several exploitable mechanisms for ion separation, both in the anode and cathode.[18,19] Examples of these mechanisms include differences in ion size,[20] valence,[21,22] shape,[20,23] and micropore surface chemistry.[23,24]

A common parameter used to quantitatively compare the ion selectivity of different systems is the separation factor β, which can be calculated from the initial ion concentrations in the feedwater and the total ions electrosorbed onto the electrodes as follows:

$$\beta^{Na^+}_{Ca^{2+}} \equiv \frac{c_{feed,Ca^{2+}}}{c_{feed,Na^+}} \frac{\Gamma_{Na^+,ads}}{\Gamma_{Ca^{2+},ads}} \quad (1)$$

If the value of $\beta^{Na^+}_{Ca^{2+}} > 1$, it indicates that the CDI system is monovalent selective. Indeed, previous studies have explored the potential of CDI cells to achieve at least partial monovalent cation (Na^+) selectivity.[25] Our group has previously investigated the use of chemical functionalization of microporous carbon electrodes to promote such selectivity.[23] For instance, Guyes *et al.* demonstrated monovalent cation selective adsorption using a sulfonated activated carbon cloth as a cathode in CDI, achieving a separation factor, β, of up to 1.6 from feedwater containing both mono and divalent ions.[26] In our non-symmetrical cells, chemical functionalization of the cathode's surface shifted the potential of zero charge (PZC) of the anode. The introduced sulfonic acid groups provide a negative chemical charge on the cathode's surface, which, due to electrical connectivity, induced a negative electronic charge on the unfunctionalized (called pristine) anode. This phenomenon caused the anode to store cations even in the absence of an applied voltage.[27] Such functionalization also resulted in a higher Ca^{2+} rejection relative to Na^+ storage at the anode during early charging times, which, combined with the storage of Na^+ ions at the cathode, led to an overall enhanced monovalent cation selectivity.

Beyond chemically functionalized microporous carbon electrodes, other strategies to achieve monovalent cation selective CDI have been explored, including the use of ultramicroporous carbons and ion-selective intercalation materials. For instance, hierarchical carbon aerogel monolith (HCAM) electrodes, characterized by a predominance of ultramicropores (sub-1 nm), exhibited high selectivity for Na^+ over Ca^{2+} with good separation factors.[25] This selectivity was attributed to a reduced affinity for Ca^{2+} within the smaller pores while applying higher voltages. Zhang *et al.* employed ultramicroporous activated carbon cloth with a narrow pore size distribution to preferentially adsorb Na^+ from a pool of monovalent and divalent cations, achieving a $\beta^{Na^+}_{Ca^{2+}}$ of 6.25.[15] Certain intercalation materials, such as Prussian blue analogues (PBA), have also been used for the selective adsorption or insertion of cations in their interstitial lattice structures within CDI cells.[28] One such study used a CDI cell with two nickel hexacyanoferrate (NiHCF) electrodes separated by an anion exchange membrane (AEM) and reported $\beta^{Na^+}_{Mg^{2+}} \approx 17$.[29] Subsequent research indicated that Na^+ ions possess lower absorption energy compared to divalent cations on NiHCF, favoring Na^+ uptake.[30] Other monovalent-selective separation techniques involve the use of monovalent ion-selective membranes (MISM), where the separation is driven by a combination of pressure and the electric field gradient. Shi *et al.* integrated a MISM into a CDI system for separating Li^+ from Mg^{2+}, achieving a separation factor of 2.95.[31] Table S3 in the ESI summarizes the parameters for all these different strategies used to achieve selectivity in CDI.

Here, we introduce the phosphorylation of microporous carbon electrodes, which, when implemented as the cathode in conjunction with a pristine carbon anode, achieves unparalleled selectivity for Na^+ over Ca^{2+} in a flow-through electrode CDI. Compared to our previous work utilizing sulfonated cathodes,[26] which already exhibited some monovalent selectivity ($\beta^{Na^+}_{Ca^{2+}} = 1.6$), the phosphoric acid functional groups are bulkier, carry higher negative surface charge and are also electrochemically stable, which should lead to higher selectivity.[20] As described above, a CDI cell incorporating such a phosphorylated cathode leverages a combination of mechanisms to achieve unprecedented monovalent cation selectivity, particularly after optimizing the electrical parameters of both charging and discharging steps. We demonstrate that by employing short cycle times (6 minutes), we can achieve perfect selectivity towards Na^+ absorption across a broad range of operational parameters, namely removing Na^+ without removing any Ca^{2+}. Specifically, using a water feed solution containing 17.4 mM Na^+ and 2.1 mM Ca^{2+}, we achieve a Na^+ removal of up to 160 μmol g^{-1} of electrode, with no Ca^{2+} removal. This perfect selectivity is achieved with remarkably low energy consumption, as low as 0.28 kWh m^{-3}. This research paves the way for breakthrough monovalent cation selective separations using CDI with readily available electrode materials and chemicals.

Results and discussion

In our previous investigations into CDI cells employing sulfonated cathodes, monovalent cation selectivity with a separation factor ($\beta^{Na^+}_{Ca^{2+}}$) of up to 1.6 was obtained.[23,26] Modelling studies suggest that increasing the concentration of negatively

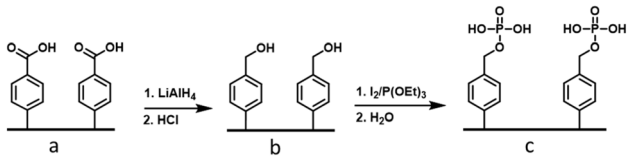

Scheme 1 Surface chemical modification of the oxidized microporous carbon sheet (a); after reduction (b), and the phosphorylation process (c). Note that oxidized graphite has additional types of carboxylic acids and alcohols; the scheme is just a general representation of the reduction of carboxylic acids to alcohols, which combined with those already in the material, get phosphorylated in the second step.

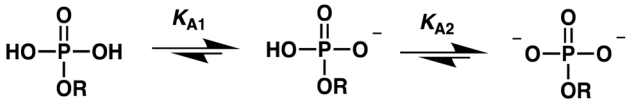

Scheme 2 Deprotonation of an organic phosphoric acid.

charged chemical groups (σ_{chem}) in the cathode could improve such selectivity.[20,27] One approach to achieve a higher surface negative charge concentration is to employ chemical groups with higher valence than the monovalent sulfonate groups. In this work, we introduce organophosphoric acid as the functional group within the carbon micropores. Phosphate functional groups offer several potential advantages: a larger steric volume,[32] a potentially higher valence (see Scheme 2 below), and superior electrochemical stability compared to sulfonate groups.[33,34] Consequently, this unsymmetrical CDI cell configuration featuring electrodes with different mass and surface charge characteristics presents a novel avenue for achieving CDI with enhanced monovalent selectivity.

When considering methodologies for carbon material phosphorylation, a review of the literature revealed that, to the best of our knowledge, no protocol was established for directly functionalizing graphitic carbon materials' surfaces with phosphoric acid groups.[35–37] However, promising approaches for phosphorylating the surface of nanodiamonds were found.[38] These were used to improve their oxidative stability, a property also desirable for graphitic carbon electrodes. The method reported by Presti *et al.* starts from the surface oxidation to introduce oxygen-containing functional groups such as alcohols and carboxylic acids, followed by direct phosphorylation with phosphoryl chloride ($POCl_3$). To evaluate this synthetic method in our materials, we employed a previously developed nitric acid surface oxidation procedure for pristine carbon electrodes,[39] known to effectively introduce the same oxygen functional groups as reported in the nanodiamond study. After confirming successful oxidation, reaction with $POCl_3$ was done in dichloromethane (CH_2Cl_2). After washing and drying, the resulting material was subjected to elemental analysis using inductively coupled plasma (ICP) and energy-dispersive X-ray spectroscopy (see the ESI). However, neither technique detected reasonable amounts of phosphorus on the carbon surface.

We returned to the literature looking for alternative protocols to synthesize organophosphoric acids from alcohols. Stowell *et al.* described a methodology using iodine (I_2) to activate trialkyl phosphites, enhancing their electrophilicity.[40] This method was reported to be effective for both aliphatic alcohols and phenols. As described in Scheme 1, our approach started with the nitric-acid oxidized carbon electrodes (a), which were subjected to hydrogenation with lithium aluminum hydride ($LiAlH_4$). This step aimed at converting all the carboxylic acids into additional alcohol functional groups, as confirmed by IR spectroscopy (see Fig. S2). Then, the hydrogenated carbon material was introduced into a flask to which a solution of triethyl phosphite ($P(OEt)_3$) activated by I_2 in CH_2Cl_2 was added to induce the phosphorylation of the alcohol groups (c). After washing and drying, the material was analyzed by ICP, which revealed a phosphorus content of 3.53 mass weight percent, indicating a significant surface functionalization (Fig. 1). Scanning electron microscopy (SEM) analysis showed no significant alterations in the carbon material's morphology, although a few black spots appear which may represent the remaining organic material (Fig. 1). Notably, the pore volume of the carbon material, as determined by nitrogen adsorption using BET analysis, remained fairly constant during the entire surface modification process (see Fig. 1 and S1).

To further corroborate and characterize the carbon material surface chemical functionalization, IR spectroscopy was performed (Fig. 2 and S2). Comparison of the spectrum of the phosphorylated material with that of the pristine carbon electrode, which consists mostly of carbon–carbon single and double bonds, revealed the emergence of several new characteristic peaks. These include peaks indicative of P–O and P=O bonds, as well as the presence of O–H stretching vibrations and even a weak C–H stretching band, which is probably a consequence of full hydrogenation of carboxylic acids. X-ray

Sample	Pore volume [cm³/g]	ICP%			
		C	H	O	P
Pristine	0.56	97.83	0.90	0.79	<0.01
Phosphorylated	0.49	86.72	1.78	7.29	3.53

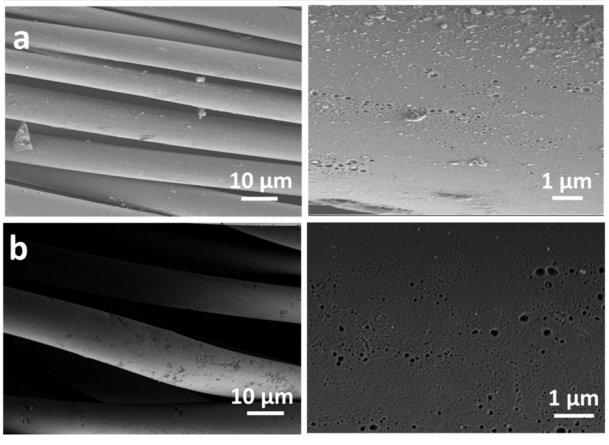

Fig. 1 SEM images of the pristine sheet before (a) and after phosphorylation (b). Pore volume measured by BET (see the ESI) and weight percentage values for C, H, O and P elements from ICP of pristine carbon and phosphorylated electrodes.

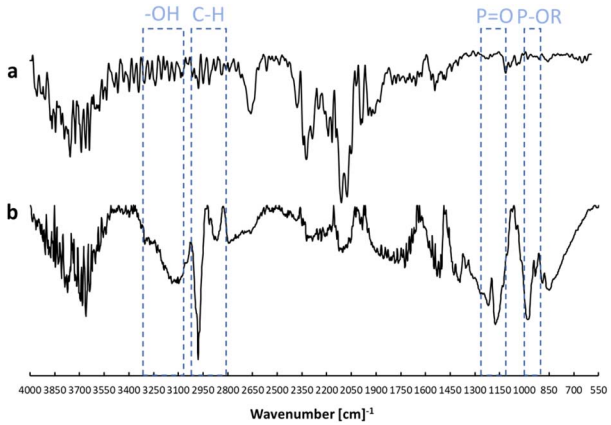

Fig. 2 IR spectroscopy measurements of the pristine sheet before (a) and after phosphorylation (b).

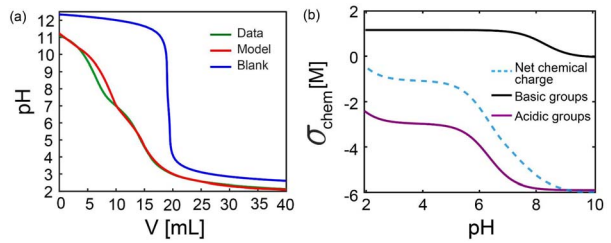

Fig. 3 (a) Results of model-to-data fitting, showing experimental titration data (green) and micropore EDL theory results (red) for the unused phosphorylated material. Also shown is the blank titration without any carbon material (blue). (b) Chemical surface charge concentration and σ_{chem} of the phosphorylated material, obtained from model-to-titration data fitting.

photoelectron spectroscopy (XPS) analysis further confirmed the presence of P═O and P–O–C but the absence of inorganic phosphorus (see Fig. S5).

To quantify the concentration of acidic functional groups introduced onto the carbon material's surface, a direct titration of the carbon in a basic solution was carried out (Fig. 3). As shown in Fig. 3a, the equilibrium pH during the direct titration varies as a function of the volume of strong acid titrant added (V). The blank titration, performed on the base solution (0.05 M NaOH) without any carbon sample (blue curve), commenced at pH = 12 and reached the expected equivalence point at $V = 20$ ml, consistent with the concentrations and quantities of the strong acid and base solutions. In contrast, the titration curve of the phosphorylated electrode (green curve) displayed a significant leftward shift relative to the blank. It began at a lower initial pH of about 11 at $V = 0$ ml, and reached its equivalence point at pH = 7 after only *ca.* $V = 10$ ml titrant was added. This substantial shift relative to the blank titration curve provides strong evidence for the presence of a high concentration of acidic functional groups on the phosphorylated carbon material.

To determine the micropore concentration of acidic groups, and considering the diprotic nature of the organophosphoric acid with distinct pK_a values, we developed a suitable model to use for fitting to the titration data (see the Theory section below). The fitted model titration curve (red curve in Fig. 3a) demonstrates an overall good agreement with the experimental data. The pK_a values of the acidic groups were used as constrained fitting parameters, yielding values of 1.6 and 6.5, along with a pK_a of 8.3 for a weak base site.[41] Fig. 3b shows the calculated micropore chemical charge concentration (σ_{chem}) of the phosphorylated carbon material as a function of pH, derived from this model fitting. The results indicate a high concentration of acidic sites of 2.8 M (corresponding to a total charge concentration of $\sigma_{chem} = 5.6$ M at high pH), as well as a weak base concentration of 1.6 M. The acid charge concentrations obtained with this phosphorylation protocol are notably higher than those reported for oxidized and sulfonated carbon materials in previous studies by Guyes *et al.* and Uwayid *et al.*[23,42] The net chemical charge concentration curve (blue dashed line in Fig. 3b) reveals that the micropores of the phosphorylated carbon material exhibit a net negative charge across the entire pH range investigated.

Having successfully prepared the phosphorylated electrode, we integrated it as the cathode in a CDI cell and conducted initial testing of its electrochemical performance through 11 charge/discharge cycles. This initial investigation focused on the cell's current and effluent ionic conductivity dynamics when paired with a pristine anode. The CDI cell was operated under the following conditions: a synthetic feedwater solution containing 17.4 mM NaCl + 2.1 mM $CaCl_2$ was supplied at a flow rate of 1 ml min^{-1}. During the charging step, a constant voltage of 0.8 V was applied, followed by a discharge voltage of −0.6 V, with each step lasting 3 min (6 min per cycle).

These initial parameters were selected based on the modelling work described by Sahray *et al.*,[27] which indicated preferential Na^+ electrosorption over divalent ions at shorter charging times. This aligns with the experimental observations of Zhao *et al.*,[21] who reported that monovalent ions are initially adsorbed but are gradually displaced by divalent ions. Furthermore, Sahray *et al.*'s model also suggested that applying negative discharge voltages would enhance ion separation. Our previous work with sulfonated cathodes also employed short cycle times to achieve the desired monovalent cation selectivity.[26]

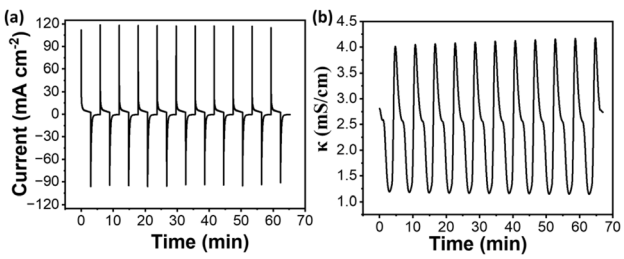

Fig. 4 Experimentally-measured cell current and effluent ionic conductivity of the CDI cell with a phosphorylated cathode and pristine anode: (a) cell current during 11 charge/discharge cycles at constant voltage, with 0.8 V charging voltage and −0.6 V discharge voltage. (b) The conductivity of the effluent measured simultaneously with the charge/discharge process shown in (a).

Fig. 4a shows the current response during the 11 charge/discharge cycles. As the charging process begins, a characteristic current spike is observed, corresponding to the rapid formation of the electrical double layer (EDL) as ions are electrosorbed onto the electrode surfaces. Subsequently, the current decays to a steady-state value as the EDL approaches saturation and equilibrium is established within the cell. Upon transitioning to the negative discharge voltage, an inverted current spike is evident. This transient surge in current arises from the cell's response to the abrupt voltage change. The conductivity of the effluent was measured simultaneously (Fig. 4b) and shows a similar trend, showing a reduction while ions are electrosorbed (charging) along with a fast release of the ions upon discharging.

Given the apparent stability of the CDI system and observation that current and conductivity approach near-dynamic steady-state under the initial conditions, we proceeded to optimize the discharge voltage. Fig. 5 shows the electrosorption of Na^+ and Ca^{2+} ions as a function of discharge voltage, while maintaining a constant charging voltage of 1.2 V. To quantify salt electrosorption within the micropores of our electrodes, we employed a modified Donnan model. This model presumes that ions are stored within the volume of the micropores rather than along the pore surface, leading to the assumption of a uniform electrostatic potential within the pores.[23] The electrosorption of a specific ion was calculated using the following formula:[42]

$$\Gamma_i = \frac{\Delta c_i \times V}{m} \quad (2)$$

where Γ_i is the electrosorption, Δc_i is the difference between the feed concentration, $c_{\text{feed},i}$, and the effluent concentration, $c_{\text{eff},i}$, all of the i-th ion. Also, V is the volume of the collected sample and m is the electrodes' mass.

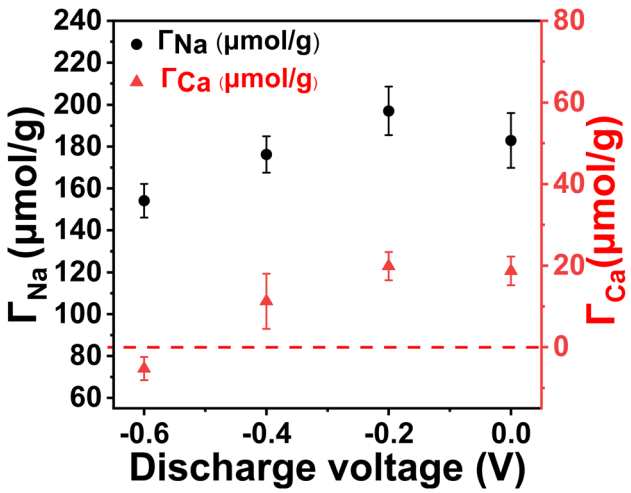

Fig. 5 Discharge voltage optimization towards higher monovalent selectivity in the CDI cell with a phosphorylated cathode and pristine anode. Electrosorption of Na^+ (left y-axis) and Ca^{2+} (right y-axis) measured after 11 cycles as a function of the discharge voltage. For all the experiments the charging voltage was 1.2 V and negative electrosorption at −0.6 V indicates perfect selectivity for Na^+ ions over Ca^{2+} ions. Error bars represent standard deviations from 4 independent repetitions.

As seen in Fig. 5, and consistent with previous modeling predictions,[27] the discharge voltage plays a crucial role in the overall extent of ion electrosorption, as well as the CDI cell ion-selectivity. As the discharge voltage changes from 0 to −0.6 V, the overall electrosorption of ions (encompassing both Na^+ and Ca^{2+}) first exhibits a slight increase, peaking at −0.2 V, before subsequently declining. Notably, at a discharge voltage of −0.6 V, the CDI cell presents negative Ca^{2+} electrosorption, *i.e.*, desorption of divalent ions. This negative electrosorption of Ca^{2+} is indicative of perfect monovalent selectivity. Under these specific operating conditions, the electrodes effectively remove only Na^+ ions from the feedwater, resulting in an effluent stream with an even slightly elevated Ca^{2+} concentration relative to the feed. This implies that during the charging step, the electrodes release more Ca^{2+} ions from the micropores than they adsorb. With $\Gamma_{Ca^{2+}} = 0$ in this discharge voltage, the value of $\beta^{Na^+}_{Ca^{2+}}$ tends to infinity, making this CDI cell perfectly monovalent selective.

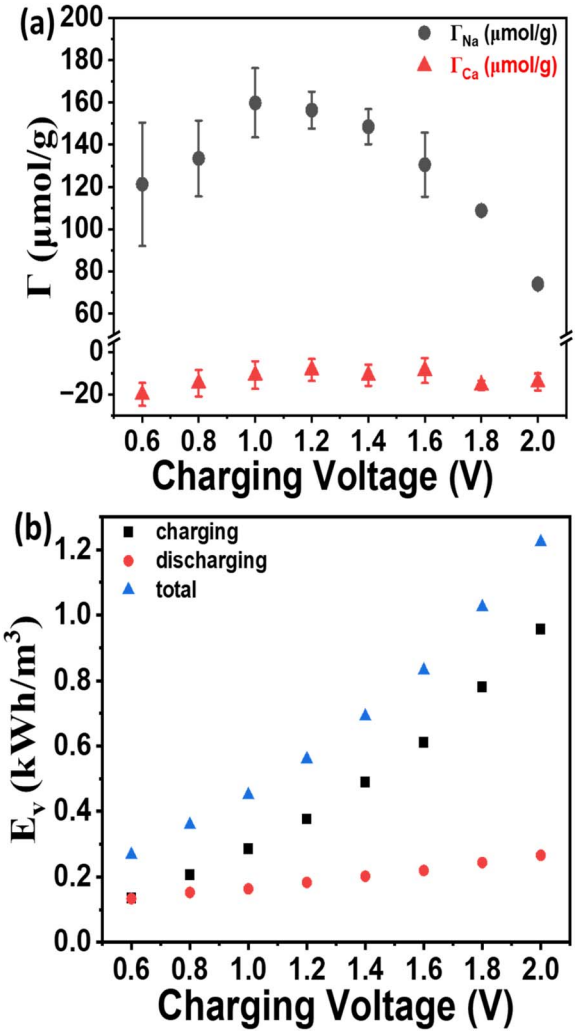

Fig. 6 Charging voltage optimization: (a) electrosorption of Na^+ (black circles) and Ca^{2+} (red triangles) as a function of charging voltage. Error bars represent standard deviations from 4 independent repetitions. (b) Energy consumption as a function of charging voltage. The discharging voltage in all the experiments was −0.6 V.

This phenomenon can be attributed to several factors. First, as described above, the organophosphoric acid groups introduce both a high local density of fixed chemical negative charges in the cathode and an induced negative charge in the anode. Before charging begins, as the cell is maintained at a negative applied potential (or is short-circuited), the negatively charged anode electrosorbs cations, with selectivity for the divalent cation, Ca^{2+}. Moreover, given the steric crowding and weak charge, these electrodes tend to adsorb Ca^{2+} even without applying voltages. Upon charging, positive charge is induced in the anode, releasing the stored Ca^{2+} ions into the water. Simultaneously, under short charging cycles and elevated cathodic potentials, the preferential electrosorption of Na^+ is both kinetically and thermodynamically favored due to its smaller hydrated radius and faster diffusion rate. This trend especially holds within the confined, negatively charged environments generated by phosphorylation. Finally, during discharging, the presence of excess repulsive electrostatic potential and ion volume exclusion interactions[20] becomes dominant at the cathode, releasing both cations. Yet, Ca^{2+} is resorbed in the anode to balance its negative charge with fewer ions. We note that, although the underlying mechanisms driving perfect monovalent selectivity are expected to be applicable to a variety of ion pairs and over a wide range of concentration ratios, a detailed analysis of these cases is outside the scope of the current study.

To partially verify this, we evaluated the charging voltage, which significantly influences both the overall electrosorption capacity and the energy consumption of the CDI process per volume of effluent. While maintaining a constant discharge voltage of −0.6 V, we varied the charging voltage from 0.6 to 2.0 V. Fig. 6a details the electrosorbed Na^+ and Ca^{2+} per weight of electrode as a function of applied voltage. One can see that perfect selectivity was maintained independently of charging voltage (*i.e.*, no Ca^{2+} removal), supporting that the Ca^{2+} desorption at short charging times is the key mechanism to achieve this selectivity. Moreover, results indicate that the maximum Na^+ electrosorption reaches nearly 159 μmol g^{-1} electrode material, at a charging voltage of around 1 V. Yet, as shown in Fig. 6b, increasing charging voltage leads to a higher energy consumption. Under the optimal operating conditions (1 V during charging and −0.6 V during discharging, 6 min per cycle), our CDI cell consumes *ca.* 0.4–0.5 kWh m^{-3}, representing a relatively low energy footprint relative to other, less selective desalination technologies such as ED (*ca.* 2.0 kWh m^{-3}) and reverse osmosis (*ca.* 2.3 kWh m^{-3}).[43,44]

Conclusions

In conclusion, we successfully prepared and implemented novel phosphorylated microporous carbon electrodes as the cathode material in a CDI cell. The introduction of negatively charged, bulky organophosphate functional groups on the cathode surface significantly shifted the point of zero charge, leading to the intriguing observation of spontaneous Ca^{2+} ion adsorption by the anode even without applied voltage. By optimizing the discharging voltage to −0.6 V, we achieved perfect monovalent cation selectivity. Under these conditions, Na^+ and Cl^- were preferentially electrosorbed during the charging step, while the pre-adsorbed Ca^{2+} was desorbed, providing an effluent with slightly higher Ca^{2+} concentration than the feedwater. Importantly, the subsequent discharging step facilitated the adsorption of additional Ca^{2+}, effectively displacing the previously adsorbed Na^+ and Cl^-. This ion-exchange mechanism (Na^+ to Ca^{2+}) allows for consistent selective removal of Na^+ over subsequent cycles. While energy is indeed consumed during both the charging and discharging steps, unlike conventional CDI cells where some energy recovery during discharge is possible, the overall energy consumption under optimal Na^+ adsorption conditions remains relatively low. This innovative electrode configuration presents a promising pathway for significant SAR reduction in water treatment, offering a valuable technology for applications such as irrigation water conditioning and wastewater treatment. Naturally, long term stability of such devices and electrodes needs to also be tested,[38] and we plan to report such results in due time.

Materials and methods

Phosphorylation of carbon electrodes

Microporous carbon cloth (MCC-5092-15; Kynol Europa GmbH, Germany) with a thickness of ∼600 μm and a surface area of ∼1400 m^2 g^{-1} was used as an electrode material in this study. To prepare the phosphorylated electrode, this carbon cloth was initially oxidized following a previously described procedure.[39] After washing with deionized (DI) water and vacuum drying at 50 °C overnight, the oxidized carbon sheets were treated with excess $LiAlH_4$ (3 times the weight of the sheet) in anhydrous tetrahydrofuran (THF) under a N_2 atmosphere at 0 °C. The mixture was then warmed to 65–75 °C for 48 h. The reaction was quenched with ice-water, and the carbon sheets were subsequently soaked in concentrated HCl (32 vol%) twice to remove aluminum salts, followed by three washes with DI water and vacuum drying. This hydrogenated carbon sheet (see the ESI) was then phosphorylated with a pre-prepared phosphorylating solution. The phosphorylating agent was synthesized by adding iodine (1.5 g, 1.1 equivalents) to a triethylphosphite (1 ml, 1.2 equivalents) solution in anhydrous CH_2Cl_2 (5.0 ml) at 0 °C. After 5 minutes, the clear, colorless solution was allowed to warm to 25 °C. The phosphorylating agent was then added dropwise, over a period of 10–15 minutes, to a flask containing the carbon sheets (0.26 g) and pyridine (2.5 ml, 4.0 equivalents) in anhydrous CH_2Cl_2 (25.0 ml). The mixture was refluxed for 48 h under light stirring. Finally, the phosphorylated carbon sheets were removed, washed three times by soaking in DI water for 15 min each, and dried under vacuum (Scheme 1). The material was then characterized by infrared (IR) spectroscopy, scanning electron microscopy (SEM) and acid–base titration, as described below.

Characterization of surface functionalization

To verify and quantify the surface functional groups, the MCC carbon material (0.4 g) was ground into a powder and immersed in a bottle containing NaOH (0.05 M, 20 ml), which was presparged with N_2 for 20 min under stirring. The bottle was

sealed with parafilm and then agitated for 24 h to ensure equilibrium was reached. Then, the solution was transferred to an automated titration vessel (904 Titrando Metrohm AG, Switzerland), sealed, and purged with N_2 for an additional 20 min before initiating the automatic titration with 0.05 M HCl. Blank titrations, performed using the same procedure but without the addition of a carbon material, were conducted to account for any background effects.

CDI experimental setup

A lab-scale CDI system was constructed, comprising a feedwater reservoir (0.5 l) connected to a custom-built CDI cell *via* a peristaltic pump (Masterflex, Cole-Parmer, USA) using flexible tubing (Scheme S1). A contactless conductivity sensor (TraceDec 390, Innovative Sensor Technologies GmbH, Austria) was positioned downstream of the CDI cell to continuously monitor effluent conductivity. A power source (Keithley Instruments 2400, USA) was used to apply voltage across the electrodes within the CDI cell. The peristaltic pump and the power source were controlled using custom MATLAB scripts. Feedwater was pumped from the reservoir through the CDI cell and the conductivity sensor. The effluent was collected in vials for further analysis. The CDI cell was configured such that the feedwater entered through the cathode and exited through the anode. In addition, there is a small pyramidal reservoir of around 0.5 ml in the cathode end plate for controlling the pressure drop in the cell. Following process optimization, as described below, the standard operating parameters included a flow rate of 1 ml min^{-1} and charge/discharge steps that last 3 min each. Effluent samples were collected and evaluated for pH, Ca^{2+} ion concentration, and conductivity after 11 cycles of operation.

CDI cell setup

The CDI cell was constructed using two square MCC electrodes (2.25 cm × 2.25 cm), each of ~600 μm thickness. The cathode consisted of the phosphorylated MCC material, while the anode was made from pristine MCC. The two electrodes were separated by a thin PTFE separator (Omnipore, pore size 0.45 μm) to prevent electrical short-circuiting. Each electrode was in direct contact with a graphite-based current collector for optimal electrical connection to the power source. The current collectors featured a 9 × 9 grid of 1.5 mm diameter holes for efficient feedwater passage and two extensions for external electrical connections. The CDI cell was housed between two acrylic end plates. The upstream end plate incorporated a pyramidal reservoir of ~0.5 ml to manage the pressure drop across the cell.

Theory

In order to interpret our direct titration results, following our previous studies on a sulfonated carbon electrode,[26] we used a titration model which includes a single weak base group, B, and a single diprotic acid group, A. We here use the subscript A_1 for the first protonation reaction and A_2 for the second, with equilibrium constants defined as

$$K_{A1} = \frac{c_{HA^-} \cdot c_{mi,H^+}}{c_{H_2A}},\quad K_{A2} = \frac{c_{A^{-2}} \cdot c_{mi,H^+}}{c_{HA^-}},\quad K_B = \frac{c_B \cdot c_{mi,H^+}}{c_{BH^+}}. \quad (3)$$

The concentrations c_{HA^-}, $c_{A^{-2}}$ and c_B are for both deprotonated forms of species A and the deprotonated species B, respectively, while c_{mi,H^+} is the micropore hydronium ion concentration. Also, c_{BH^+} and c_{H_2A} are the concentrations of the protonated form of B and A, respectively. The model assumes an electrically uncharged electrode ($\sigma_{elec} = 0$) with micropore volume v_{mi}. The reference conditions consider an electrode soaked in a strong base solution of NaOH with volume V_0, and with this solution titrated with an HCl solution of volume V. The mass conservation of Na and Cl, when applying a modified Donnan EDL model,[21,45,46] yields, respectively,

$$V_0 c_{NaOH} = (V_0 + V - m v_{mi}) c_{Na^+} + m v_{mi} c_{Na^+} e^{-\Delta\phi_D} \quad (4)$$

$$V c_{HCl} = (V_0 + V - m v_{mi}) c_{Cl^-} + m v_{mi} c_{Cl^-} e^{\Delta\phi_D} \quad (5)$$

where $\Delta\phi_D$ is the electrode's Donnan potential, m is the electrode mass, and c_{Na^+} and c_{Cl^-} are Na^+ and Cl^- ion bulk concentrations, respectively. We can write solution electroneutrality, for the case where the concentration of OH^- ions (in units of mM) is represented by $\frac{K_w}{10^{3-pH}}$, and K_w is the water dissociation constant, as

$$\sum z_i c_i = c_{Na^+} + 10^{3-pH} - c_{Cl^-} - \frac{K_w}{10^{3-pH}} = 0 \quad (6)$$

As we assumed $\sigma_{elec} = 0$, the micropore charge balance is

$$\sigma_{ionic} + \sigma_{chem} = 0 \quad (7)$$

where the ionic charge is calculated by employing the Donnan condition, resulting in

$$\sigma_{ionic} = -2(c_{Na^+} + c_{H^+})\sinh(\Delta\phi_D) \quad (8)$$

and the micropore chemical charge by definition

$$\sigma_{chem} = F\sum z_i c_{chem,i} = F(c_{BH^+} - c_{HA^-} - 2c_{A^{2-}}). \quad (9)$$

Rewriting c_{BH^+}, c_{HA^-}, and $c_{A^{2-}}$ as a function of the dissociation constants, micropore H^+ concentration, c_{mi,H^+}, and the total concentrations of the different chemical groups, eqn (9) can be rewritten as

$$\sigma_{chem} = F\left(\frac{c_{mi,H^+}}{c_{mi,H^+} + K_B} c_{B,t} - \frac{K_{A1} c_{mi,H^+}}{c_{mi,H^+}^2 + K_{A1} c_{mi,H^+} + K_{A2}K_{A1}} c_{A,t} - 2\frac{K_{A2}K_{A1}}{c_{mi,H^+}^2 + K_{A1} c_{mi,H^+} + K_{A2}K_{A1}} c_{A,t}\right) \quad (10)$$

where $c_{A,t}$ and $c_{B,t}$ are the total group concentrations of the acidic and basic groups, respectively, which include both the protonated and deprotonated forms.

Eqn (3)–(10) are solved simultaneously using K_{A1}, K_{A2}, K_B, $c_{A,t}$ and $c_{B,t}$ as fitting parameters to obtain fits to the experimental

titration curves. K_{A1} is restricted to the range of 10^{-1} to 10^{-2} and K_{A2} is restricted to the range of $10^{-5.5}$ to 10^{-7}, according to the values for phosphoryl groups reported by Shamir *et al.*[41]

Conflicts of interest

There are no conflicts to declare.

Data availability

The data supporting this article have been included as part of the SI.

Supplementary information gives details on the materials and analytical equipment used; characterization data (ICP and BET data, IR, SEM, EDS, XPS spectra for the different steps in the electrode preparation); CDI numeric data and statistical analysis; and ion-selectivity comparison of this work with previously developed CDI strategies. See DOI: **https://doi.org/10.1039/d5ta05182g**.

Acknowledgements

We would like to acknowledge the Israel Innovation Authority (grant number 77640) for funding this project. S. N. acknowledges the Neubauer Family Foundation for the "Neubauer Doctoral Fellowship". R. U. acknowledges the Ariane de Rothschild Women Doctoral Program for the Doctoral Fellowship.

Notes and references

1 S. Kim, D. S. Han and H. Park, *Energy Environ. Sci.*, 2024, **17**, 4488–4497.
2 Y. Ha, H. Lee, H. Yoon, D. Shin, W. Ahn, N. Cho, U. Han, J. Hong, N. Anh Thu Tran, C. Y. Yoo, H. S. Kang and Y. Cho, *Sep. Purif. Technol.*, 2021, **254**, 117500.
3 A. Kumar, Y. Kim, X. Su, H. Fukuda, G. Naidu, F. Du, S. Vigneswaran, E. Drioli, T. A. Hatton and J. H. Lienhard, *Trends Chem.*, 2021, **3**, 819–831.
4 J. G. Gamaethiralalage, K. Singh, S. Sahin, J. Yoon, M. Elimelech, M. E. Suss, P. Liang, P. M. Biesheuvel, R. L. Zornitta and L. C. P. M. De Smet, *Energy Environ. Sci.*, 2021, **14**, 1095–1120.
5 J. Choi, H. Lee and S. Hong, *Desalination*, 2016, **400**, 38–46.
6 A. N. Shocron, R. S. Roth, E. N. Guyes, R. Epsztein and M. E. Suss, *Environ. Sci. Technol. Lett.*, 2022, **9**, 889–899.
7 J. Ma, Q. Li, X. Zhang and F. Yu, *Coord. Chem. Rev.*, 2024, **517**, 216001.
8 P. Ren, B. Wang, J. G. de Andrade Ruthes, M. Torkamanzadeh and V. Presser, *Desalination*, 2024, **592**, 118161.
9 Y. Horowitz, C. Schmidt, D. Yoon, L. M. Riegger, L. Katzenmeier, G. M. Bosch, M. Noked, Y. Ein-Eli, J. Janek, W. G. Zeier, C. E. Diesendruck and D. Golodnitsky, *Energy Technol.*, 2020, **8**, 2000580.
10 A. Al-Nahari, S. Li and B. Su, *Sep. Purif. Technol.*, 2022, **291**, 120947.
11 M. Mossad, W. Zhang and L. Zou, *Desalination*, 2013, **308**, 154–160.
12 J. Ying, Y. Lin, Y. Zhang, Y. Jin, H. Matsuyama and J. Yu, *Chem. Eng. J.*, 2022, **446**, 137076.
13 R. W. Baker, *Membrane Technology and Applications*, Wiley, Chichester, UK, 3rd edn, 2012.
14 A. W. Mohammad, Y. H. Teow, W. L. Ang, Y. T. Chung, D. L. Oatley-Radcliffe and N. Hilal, *Desalination*, 2015, **356**, 226–254.
15 Y. Zhang, P. Ren, L. Wang, E. Pameté, S. Husmann and V. Presser, *Desalination*, 2022, **542**, 116053.
16 L. Zou, L. Li, H. Song and G. Morris, *Water Res.*, 2008, **42**, 2340–2348.
17 S. Kumar, N. M. Aldaqqa, E. Alhseinat and D. Shetty, *Angew. Chem., Int. Ed.*, 2023, **62**, 202302180.
18 K. Sun, M. Tebyetekerwa, C. Wang, X. Wang, X. Zhang and X. S. Zhao, *Adv. Funct. Mater.*, 2023, **33**, 2213578.
19 H. Sharifpour, F. Hekmat, S. Shahrokhian and L. Pan, *J. Mater. Chem. A*, 2024, **12**, 31329–31346.
20 M. E. Suss, *J. Electrochem. Soc.*, 2017, **164**, E270–E275.
21 R. Zhao, M. van Soestbergen, H. H. M. Rijnaarts, A. van der Wal, M. Z. Bazant and P. M. Biesheuvel, *J. Colloid Interface Sci.*, 2012, **384**, 38–44.
22 Z. Chen, H. Zhang, C. Wu, Y. Wang and W. Li, *Desalination*, 2015, **369**, 46–50.
23 E. N. Guyes, T. Malka and M. E. Suss, *Environ. Sci. Technol.*, 2019, **53**, 8447–8454.
24 J. Yang, L. Zou and N. R. Choudhury, *Electrochim. Acta*, 2013, **91**, 11–19.
25 M. R. Cerón, F. Aydin, S. A. Hawks, D. I. Oyarzun, C. K. Loeb, A. Deinhart, C. Zhan, T. A. Pham, M. Stadermann and P. G. Campbell, *ACS Appl. Mater. Interfaces*, 2020, **12**, 42644–42652.
26 E. N. Guyes, A. N. Shocron, Y. Chen, C. E. Diesendruck and M. E. Suss, *npj Clean Water*, 2021, **4**, 1–11.
27 Z. Sahray, A. N. Shocron, R. Uwayid, C. E. Diesendruck and M. E. Suss, *Water Res.*, 2023, **246**, 120684.
28 K. Singh, Z. Qian, P. M. Biesheuvel, H. Zuilhof, S. Porada and L. C. P. M. de Smet, *Desalination*, 2020, **481**, 114346.
29 K. Singh, S. Sahin, J. G. Gamaethiralalage, R. L. Zornitta and L. C. P. M. de Smet, *Chem. Eng. J.*, 2022, **432**, 128329.
30 Y. Bao, J. Hao, S. Zhang, D. Zhu and F. Li, *Small*, 2023, **19**, 2300384.
31 W. Shi, X. Liu, C. Ye, X. Cao, C. Gao and J. Shen, *Sep. Purif. Technol.*, 2019, **210**, 885–890.
32 M. Adnan, S. J. Khan, K. Manzoor and N. P. Hankins, *Process Saf. Environ. Prot.*, 2019, **127**, 133–140.
33 G. Kilinççeker, B. Yazici, A. B. Yilmaz and M. Erbil, *Br. Corros. J.*, 2002, **37**, 23–30.
34 J. Li, A. Wang, C. Tan, D. Wu, M. Fan, K. Sun, J. Jiang, S. Boles, B. Li and J. Liu, *J. Mater. Chem. A*, 2024, **12**, 3111–3121.
35 L. Nayak, M. Rahaman and R. Giri, in *Carbon-Containing Polymer Composites*, 2019, vol. 16, pp. 65–98.
36 Y. Shen and Y. Zhu, *J. Mater. Chem. A*, 2024, **12**, 6211–6242.
37 X. Pan, J. Ji, N. Zhang and M. Xing, *Chin. Chem. Lett.*, 2020, **31**, 1462–1473.

38 C. Presti, J. G. Alauzun, D. Laurencin and P. H. Mutin, *Chem. Mater.*, 2013, **25**, 2051–2055.
39 R. Uwayid, C. E. Diesendruck and M. E. Suss, *Environ. Sci.: Water Res. Technol.*, 2022, **8**, 949–956.
40 J. K. Stowell and T. S. Widlanski, *Tetrahedron Lett.*, 1995, **36**, 1825–1826.
41 D. Shamir, I. Zilbermann, E. Maimon, A. I. Shames, H. Cohen and D. Meyerstein, *Inorg. Chim. Acta*, 2010, **363**, 2819–2823.
42 R. Uwayid, E. N. Guyes, A. N. Shocron, J. Gilron, M. Elimelech and M. E. Suss, *Water Res.*, 2022, **210**, 117959.
43 X. Wang, S. Shan, Y. Zhang, S. Q. Shi and C. Xia, *Environ. Sci.: Water Res. Technol.*, 2024, **10**, 1034–1060.
44 T. J. Welgemoed and C. F. Schutte, *Desalination*, 2005, **183**, 327–340.
45 P. M. Biesheuvel, Y. Fu and M. Z. Bazant, *Russ. J. Electrochem.*, 2012, **48**, 580–592.
46 P. M. Biesheuvel and M. van Soestbergen, *J. Colloid Interface Sci.*, 2007, **316**, 490–499.